Polymer Chemistry

ROYAL SOCIETY OF CHEMISTRY

PAPER

View Article Online
View Journal | View Issue

Cite this: *Polym. Chem.*, 2023, **14**, 3309

Water soluble non-conjugated fluorescent polymers: aggregation induced emission, solid-state fluorescence, and sensor array applications†

Anna Jose,[a] Adithya Tharayil[a] and Mintu Porel *[a,b]

In this work, two water soluble fluorescent non-conjugated polymers have been designed and synthesized. To confer water solubility, a synthetic strategy was made to incorporate secondary amine moieties and ester linkages in the backbone, and to make it fluorescent we have attached dansyl and naphthyl moieties. The polymers exhibited solid-state fluorescence which was confirmed by solid-state fluorescence spectroscopy and microscopy. They also exhibited aggregation induced emission (AIE) behaviour in a water–DMSO mixture which was confirmed by fluorescence, quantum yield, DLS, and lifetime analysis. Furthermore, the interaction of the polymers with different metal ions was studied with the aim of using it as a sensor. Among the 15 metal ions tested, it was found that the dansyl appended polymer gave distinct signals in the absorption and emission spectra for the addition of Cu^{2+}, Co^{2+}, Ag^{+}, K^{+}, Fe^{2+} and Fe^{3+} ions. These metals also showed discrete signals in the absorption spectra along with distinguishable colour changes such as Cu^{2+} – blue, Co^{2+} – pink, Ag^{+} – purple, Fe^{2+} – dark yellow and Fe^{3+} – light yellow on their addition. Further linear discriminant analysis (LDA) was performed to see the sensor array applications of the polymer and showed a discrete sensor array output and clear separation of clusters, validating the application of the polymer as a multi-analyte sensor. The separation and identification of the metals *via* LDA was also possible in nanomolar concentrations. Moreover, our strategy for developing a fluorescent polymer is also versatile for synthesising polymers with tuneable properties for diverse applications.

Received 30th March 2023,
Accepted 23rd June 2023

DOI: 10.1039/d3py00357d

rsc.li/polymers

Introduction

Water soluble fluorescent polymers are extensively used for applications in drug delivery,[1] diagnostics and therapeutics,[2] bioimaging[3] and as probes for various biological analytes[4,5] and environmental pollutants.[6–8] This is credited to the improved solubility and photostability, and robust nature of these polymers. The techniques that are conventionally used for the synthesis of polymers employ prolonged and wearisome synthetic and purification approaches, sophisticated instrumentation, harsh solvents, elevated temperatures, high pressure, and inert atmospheres. These drawbacks have provoked massive research in this arena with the aim of developing newer strategies for the simpler synthesis of polymers. The polymers hence formed can be either (a) conjugated polymers, having extensive π aromatic building units, or (b) non-conjugated polymers that do not have extensive conjugation.[9] Among these, the conjugated polymers, in view of their π aromatic conjugation, have weak solubility in aqueous media, rendering them unfit for sensing and biomedical applications. Therefore, the emphasis in recent times has been to develop water friendly nonconjugated polymers.

The attachment of a suitable fluorophore to the polymer backbone will result in the development of polymers with potential applications towards sensing various analytes with amplified sensitivity and selectivity, fast responses, and real-time detection. Fluorescent polymeric materials that are utilised for selective detection of toxic heavy metals,[10] anions,[7,11] *etc*. have been reported by various groups. In addition to these single-sensor–single analyte systems, the sensor arrays[12–14] that discriminate multiple analytes based on the discrete response pattern are also prominent for real world applications. A sensor array based on optical measurements utilises the signals from absorption and emission spectra to provide qualitative and quantitative statistics on the type and concentration of the analytes. The sensor array provides unique response patterns in the presence of various analytes, thus

[a]*Department of Chemistry, Indian Institute of Technology Palakkad, Kerala, India. E-mail: mintu@iitpkd.ac.in*
[b]*Environmental Sciences and Sustainable Engineering Centre; Indian Institute of Technology Palakkad, Kerala, India*

† Electronic supplementary information (ESI) available. See DOI: https://doi.org/10.1039/d3py00357d

paving the way for single-sensor–multiple analyte systems. The prospect of concurrent detection of multiple analytes with excellent sensitivity validates the extensive research in the field of sensor arrays.

In this work, we have put forth strategies for the synthesis of water-soluble non-conjugated polymers by attaching (a) dansyl and (b) naphthyl derivatives as fluorescent tags. Both polymers, **D1** with a dansyl tag and **N1** with a naphthyl tag, incorporate ester linkages in the backbone alongside the secondary amines that render the system water soluble. The synthetic strategy employed here does not require high temperatures or an inert atmosphere but utilises mild reaction conditions. Both of the polymers exhibited aggregation induced emission (AIE) behaviour in a water–DMSO mixture. The AIE behaviour of fluorescence materials is extensively used for applications as sensing agents,[15–17] biomarkers,[18] drug delivery agents,[19] anti-counterfeit devices,[20] and organic light-emitting diodes (OLEDs)[21] and in photovoltaics.[22] In addition to liquid-state fluorescence, the two polymers exhibited solid-state fluorescence as well. Materials with solid-state fluorescence are ideal for overcoming unfavourable ACQ (aggregation induced quenching) effects that can arise during bioimaging applications.[23] The interaction of the sensors with various metal ions was studied *via* absorbance and emission spectral analyses and the data obtained revealed the potential of the polymer to work as a sensor array. The optical data were then converted into canonical scores *via* linear discriminant analysis (LDA). Using LDA, the clear-cut distinction and identification of six metal ions, namely, Cu^{2+}, Co^{2+}, Ag^{+}, K^{+}, Fe^{2+} and Fe^{3+} were possible. This was also possible in nanomolar concentrations, making it sensitive towards the detection of metal ions. Moreover, the addition of these metal ions to polymer **D1** produced discrete colorimetric responses: Cu^{2+} – blue, Co^{2+} – pink, Ag^{+} – purple, Fe^{2+} – dark yellow and Fe^{3+} – light yellow, making it a viable tool for easy detection of metal cations in addition to being a multi-analyte sensor array.

Results and discussion

Owing to the importance of water-soluble fluorescent polymers in the detection of environmental pollutants, we have devised strategies for the synthesis of two different polymers: (a) **D1**, with a dansyl tag and (b) **N1**, with a naphthyl tag. The synthetic scheme for this is shown in Scheme 1. The reaction started with the fluorophore, either dansyl chloride, **1a**, or 2-(bromomethyl)naphthalene, **1b**, reacting with diethanol amine, **2**, in the presence of triethylamine (TEA) as a base and dichloromethane (DCM) as a solvent to form **3a**/**3b** with terminal hydroxy groups (Scheme 1). In the next step, the hydroxy groups were functionalised by the reaction with chloroacetyl chloride to produce the chloroacetyl derivative **4a**/**4b** (Scheme 1). HPLC (high performance liquid chromatography) traces of **4a** and **4b** are shown in Fig. S1 and S2.† Later, **4a**/**4b** was taken for a polymerisation reaction with 1,3-propane diamine in an acetonitrile solvent for 12 hours at room temperature to synthesise **D1** and **N1** (Scheme 1). The obtained polymer powder was washed with ethyl acetate and acetone multiple times to remove any impurities. The polymer **D1** was obtained with a yield of 71% and **N1** was obtained with a yield of 82%. The solid obtained was then dried and utilised for photophysical studies. It is to be noted that all three steps

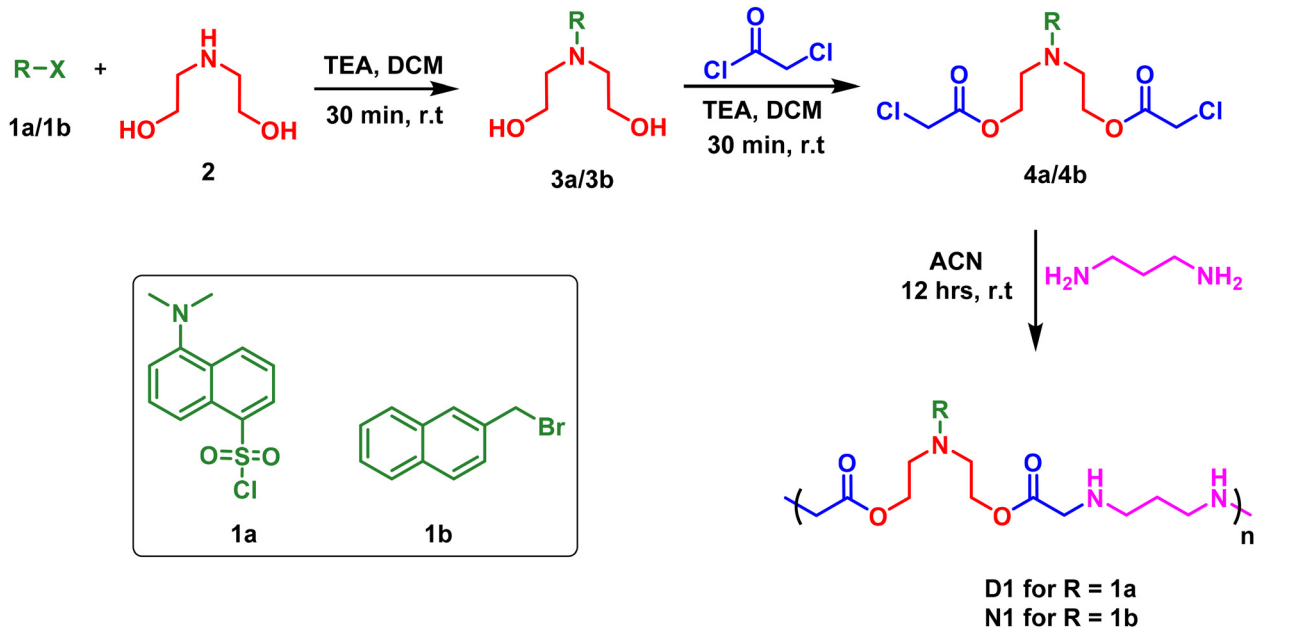

Scheme 1 The synthetic procedure for dansyl appended polymer (**D1**) and naphthyl appended polymer (**N1**). (TEA: triethylamine, DCM: dichloromethane, ACN: acetonitrile).

were performed at room temperature, using mild solvents without the need for an inert atmosphere and with inexpensive starting materials.

The molecular weight of the synthesised polymers was determined using gel permeation chromatography (GPC). For **D1** the molecular weight obtained was 18 K Da with a polydispersity index (PDI) of 1.41 (Fig. S3†). Similarly, for **N1** the molecular weight obtained was 18 K Da with a PDI of 1.22 (Fig. S4†). ^{1}H-NMR spectra of the starting materials and the polymers were also recorded (Fig. S5–S7†). The synthesised polymers were also characterised by FT-IR spectroscopy and scanning electron microscopy (SEM). The disappearance of the C–Cl stretching frequency at 785 cm^{-1} in the polymers in comparison with the precursors and the appearance of characteristic peaks of secondary amine validate the polymer formation (Fig. S8 and S9†). The surface morphology of the synthesised polymers was studied *via* scanning electron microscopy. The obtained images (Fig. S10†) indicate distinct surface morphologies for each polymer. The polymer **D1** has feather-like structures on the surface whereas the surface of **N1** is uniform and smooth. Thermal stability was studied using TG–DTA analysis (Fig. S11†). The polymer **N1** was stable up to 150 °C, and showed 50% decomposition at 300 °C and complete decomposition at 650 °C. The polymer **D1** showed 90% stability up to 125 °C. Almost 50% reduction occurred around 300 °C and complete decomposition occurred around 350 °C.

Following the synthesis, we explored the AIE (aggregation induced emission) behaviour of the polymers in the water–DMSO mixture. The synthesis of materials with AIE properties is progressing rapidly as they find use in a wide range of applications from materials science to biomedical science. In water (good solvent), both **D1** and **N1** exhibited weak emission and as the DMSO (bad solvent) fraction increased, the polymers exhibited enhanced emission due to aggregate formation. The AIE arises due to the restricted rotation of the molecules in the aggregate state, which reduces the non-radiative decay.[24–26] This is shown in Fig. 1a and b, where the increase in the percentage of DMSO from 0% to 99% resulted in enhanced fluorescence emission. The photographic images of **D1** in various water–DMSO fractions captured under a UV lamp are shown in Fig. 1c, and the AIE behaviour is also shown.

To confirm the aggregate formation, we performed a DLS (dynamic light scattering) experiment. The experiment was performed using water–DMSO mixtures with DMSO fractions of 0%, 50%, and 90% (Fig. S12 and S13†). The water–DMSO mixture of **D1** with 0% DMSO had a hydrodynamic diameter of 205.2 nm with a polydispersity index (PDI) of 0.308. For the water–DMSO mixture with 50% DMSO, the hydrodynamic diameter was 403 nm with a PDI of 0.122. For the mixture with 90% DMSO, a mix of hydrodynamic diameters was observed, with the highest value being 4472 nm (PDI 0.759). A similar experiment was done with **N1** as well. For the 0%, 50% and 90% DMSO fractions the obtained hydrodynamic diameters were 310.8 nm (PDI 0.9), 418.6 (PDI 0.275) and 661 nm (PDI 0.495), respectively. Both of these experiments clearly indicate that aggregates with larger sizes were formed in the 90%

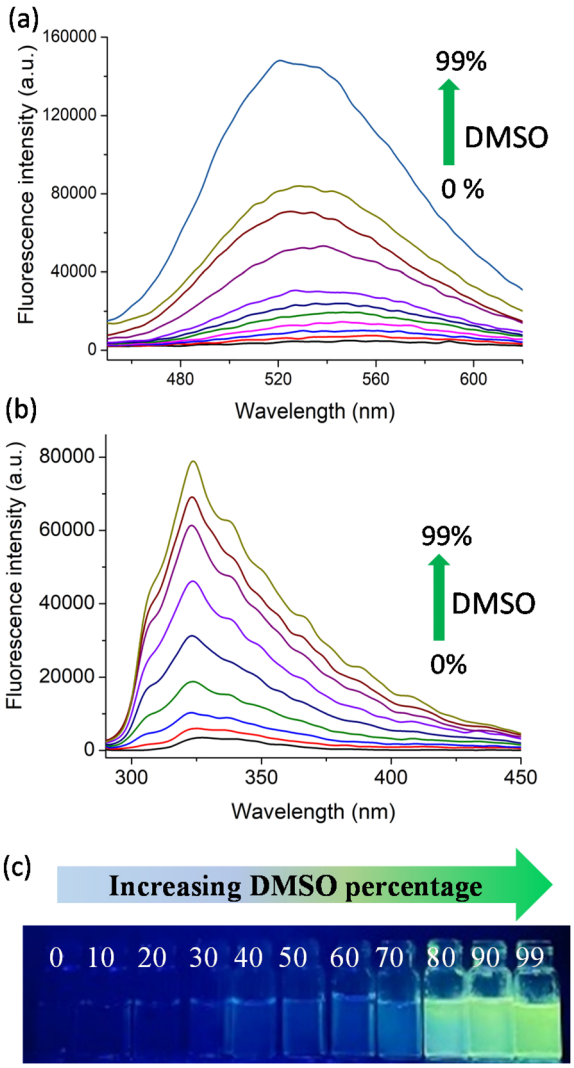

Fig. 1 The fluorescence emission intensity of (a) **D1** and (b) **N1** in a water/DMSO mixture with the DMSO fraction varied from 0% to 10%, 20%, 30%, 40%, 50%, 60%, 70%, 80%, 90% and 99% obtained with an excitation wavelength of 365 nm for **D1** and 280 nm for **N1**. (c) The photographic images of **D1** in the water/DMSO fraction showing AIE behaviour.

DMSO fraction, as observed from the fluorescence studies. This proves the aggregate formations in higher DMSO fractions.

In addition to this, the quantum yield of a few representative water–DMSO mixtures of **D1** and **N1** were determined using quinine sulphide (quantum yield, 0.54, Fig. S16†) as the reference standard. The quantum yield obtained for the 0%, 30%, 70% and 90% DMSO fractions of **D1** were 0.023, 0.061, 0.183 and 0.243 (Fig. S17†). Additionally, for the 0%, 30%, 70% and 90% DMSO fractions of **N1**, the obtained quantum yields were 0.010, 0.032, 0.113 and 0.153 (Fig. S18†). The quantum yields obtained for both polymers are shown in Table 1. In both cases, the quantum yields increased with increasing percentage of DMSO in water, which validates the formation of aggregate. The time-correlated single photon counting (TCSPC) analyses of the 30%, 60% and 90% DMSO

Table 1 Quantum yield obtained for polymers **D1** and **N1** in different DMSO fractions in water

	Quantum yield obtained for	
DMSO % in water	**D1**	**N1**
0	0.023	0.010
30	0.061	0.032
70	0.183	0.113
90	0.243	0.153

fractions of both **D1** and **N1** were used to calculate the average lifetime of the same. The fluorescence decay profiles of **D1** and **N1** are shown in Fig. S19.† The average lifetimes (τ) obtained for the 30%, 60% and 90% DMSO fractions of **D1** are 3.5 ns, 4.73 ns and 5.63 ns and those obtained for **N1** are 5.21 ns, 7.04 ns and 8.86 ns. This also indicates the aggregate formation at higher DMSO fractions.

The solid-state fluorescence and absorption spectra of the synthesised polymers **D1** and **N1** were recorded and the spectra obtained are shown in Fig. 2a and b, respectively. It can be noted that for **D1**, the excitation maximum occurred at 250 nm with a shoulder peak at 365 nm. The emission maximum for **D1** was obtained at 520 nm. For **N1** the absorption maximum was at 280 nm and the emission maximum was at 330 nm. The solid-state fluorescence images of the polymers were also obtained by viewing these polymers under UV light irradiation (Fig. 2c and d). The polymer **D1** gave bright green fluorescence whereas **N1** did not. This difference in behaviour can be attributed to the difference in the fluorescence tag present in each polymer. In addition, the images of **N1** and **D1** dissolved in 100% DMSO when viewed under a UV lamp are shown in Fig. 2e and f. respectively. The solution of **N1** is not fluorescent, whereas the solution of **D1** displays bright yellow fluorescence.

Fluorescence microscopy images of the synthesised polymers were also recorded to understand the solid-state morphology. For this, different filters that operate at different wavelengths were shone on **D1** and **N1** and the obtained images are shown in Fig. 3. The various filters used were DAPI-345/455 nm, FITC-494/518 nm, TRITC-555/580 nm, and CY3-550/565 nm with an exposure time of 200 milliseconds. The images obtained indicate that polymer **N1** shows higher emission as compared to **D1**.

Following the synthesis, characterisation and photophysical studies, we intended to use the synthesised polymers for the sensing of metal ions in water. This is important as the concentration of different metal ions in the environment and water bodies is directly connected to the quality of life of organisms and identifying the presence of these at levels above the permissible levels is required to prevent health issues. For this the excitation and emission spectra of **D1** and **N1** were recorded in aqueous media. The absorption of **D1** occurred at 365 nm and emission at 520 nm. For **N1** the excitation and emission maxima were at 280 nm and 330 nm, respectively. To understand the metal detection capacity of these polymers a 3 mg mL^{-1} solution of **D1** was prepared in water. The emission spectra of a diluted solution of **D1** were initially recorded and to this various metal solutions including Al^{3+}, Zn^{2+}, Cd^{2+}, Pb^{2+}, Fe^{2+}, Fe^{3+}, Mn^{2+}, Na^{+}, K^{+}, Co^{2+}, Cu^{2+}, Ni^{2+}, Ag^{+}, Ca^{2+} and Hg^{2+} were added. It was observed that the emission intensities underwent enhancement in the presence

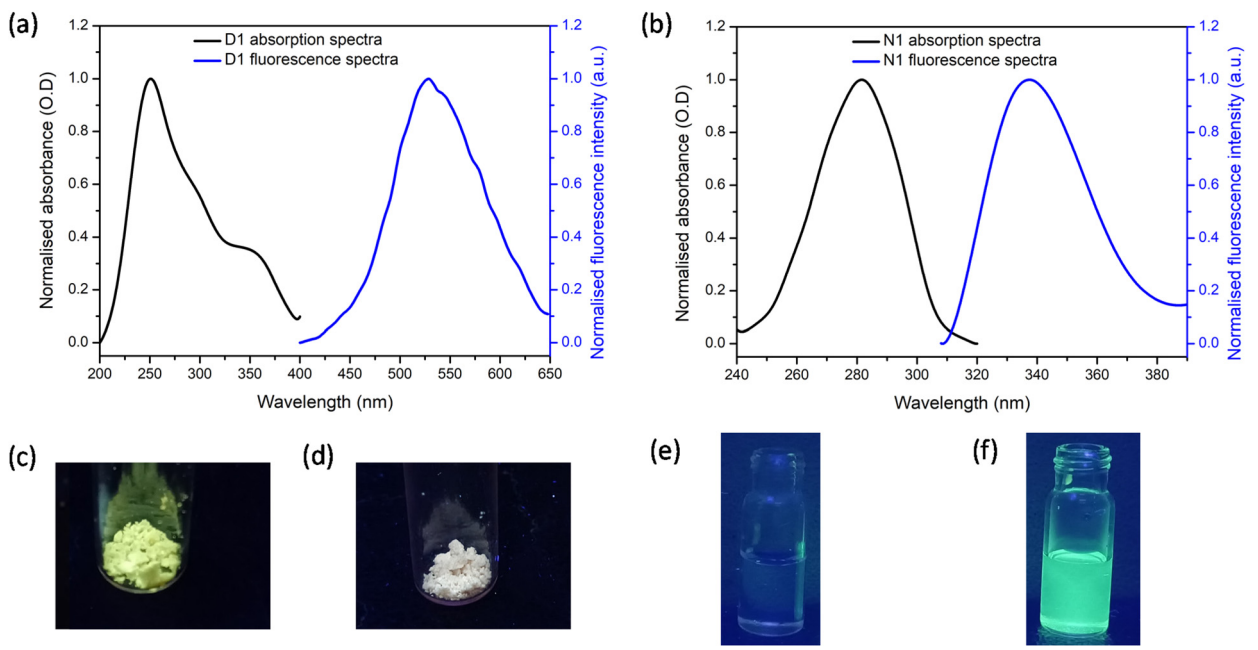

Fig. 2 The solid-state fluorescence and absorption spectra of **D1** (a) and **N1** (b) and the photographic images of **D1** (c) and **N1** (d) viewed under a fluorescent lamp. The images (e) and (f) denote **N1** and **D1** dissolved in a DMSO solution.

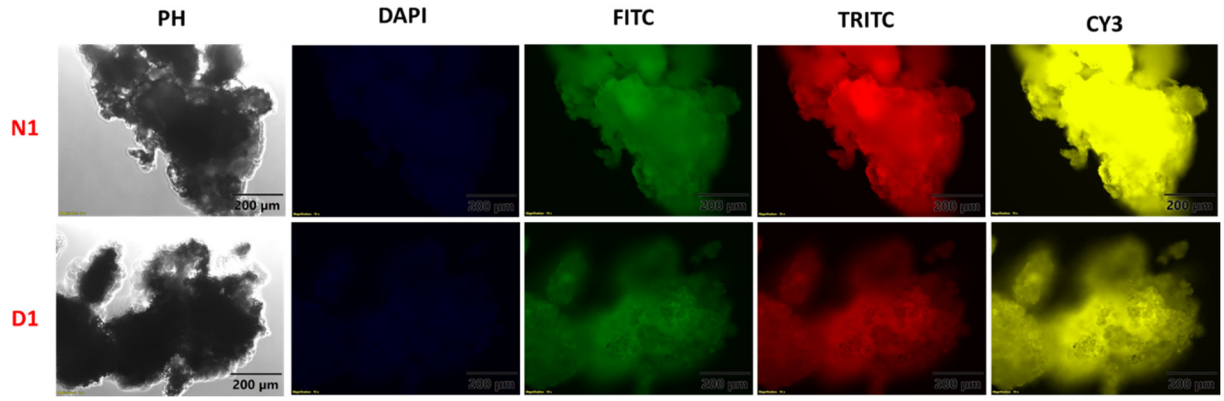

Fig. 3 Solid-phase fluorescence microscopic images of **N1** and **D1**.

of Ag^+ and K^+. For the addition of Ag^+, the emission maxima at 420 nm were found to be increasing (Fig. 4a) and for the addition of K^+, the emission maxima at 520 nm were increasing (Fig. 4a). The addition of Ag^+ ions to **D1** also resulted in aggregate formation and this was confirmed by DLS (Fig. S14†). Furthermore, the solution of **D1** + Ag^+ showed clear evidence of the Tyndall effect (Fig. S15†), demonstrating the formation of nanoscale aggregates. The addition of Cu^{2+}, Co^{2+}, Fe^{2+}, and Fe^{3+} produced quenching of fluorescence (Fig. 4a). However, the quenching observed was highest for Fe^{3+}. Furthermore, we recorded the absorption spectra of **D1** in the presence of all metal ions and found that the addition of Ag^+, Cu^{2+}, Co^{2+}, Fe^{2+}, and Fe^{3+} produced discrete colour patterns (Fig. 4b) and spectral changes (Fig. S20†). In the absorption spectra, the addition of Cu^{2+} and Co^{2+} gave absorption maxima at 670 nm and 510 nm, respectively. When Fe^{2+} and Fe^{3+} were added the absorption maxima occurred at 490 nm; nevertheless, Fe^{2+} had a higher optical density for the same amount of metal ion added. Moreover, the addition of Ag^+ gave purple, Cu^{2+} gave blue, Co^{2+} gave pink, Fe^{2+} gave dark yellow, and Fe^{3+} gave light yellow color to the **D1** solution (Fig. 4b). The same experiment was also conducted with **N1**. The fluorescence emission intensities of **N1** upon the addition of different metal ions were checked and no quenching of fluorescence for the metal ions was found (Fig. S21†).

In view of the distinct spectral patterns obtained from the absorption and emission signals of **D1** in the presence of six metal ions (Ag^+, Cu^{2+}, Co^{2+}, Fe^{2+}, Fe^{3+} and K^+), we propose to use linear discriminant analysis (LDA) to clearly discriminate these. LDA is a reduction analysis method that helps in the graphical visualisation of multidimensional data. To obtain this, triplicates of the output signals were recorded by measuring the fluorescence and absorption spectra of **D1** in the presence of Ag^+, Cu^{2+}, Co^{2+}, Fe^{2+}, Fe^{3+} and K^+ ions. From this a bar diagram of $(I_0 - I)/I_0$ for all six metals was plotted by choosing different emission and absorbance parameters (Fig. 5a). The parameters taken for consideration are F493, F510, and F420, which denote the fluorescence response patterns, and A490, A510, and A670, which denote the absorbance response patterns. From these labels, a LDA score plot was obtained and is shown in Fig. 5b. The LDA of six metal ions produced distinct clusters and high-level dispersion of data. This allowed a dis-

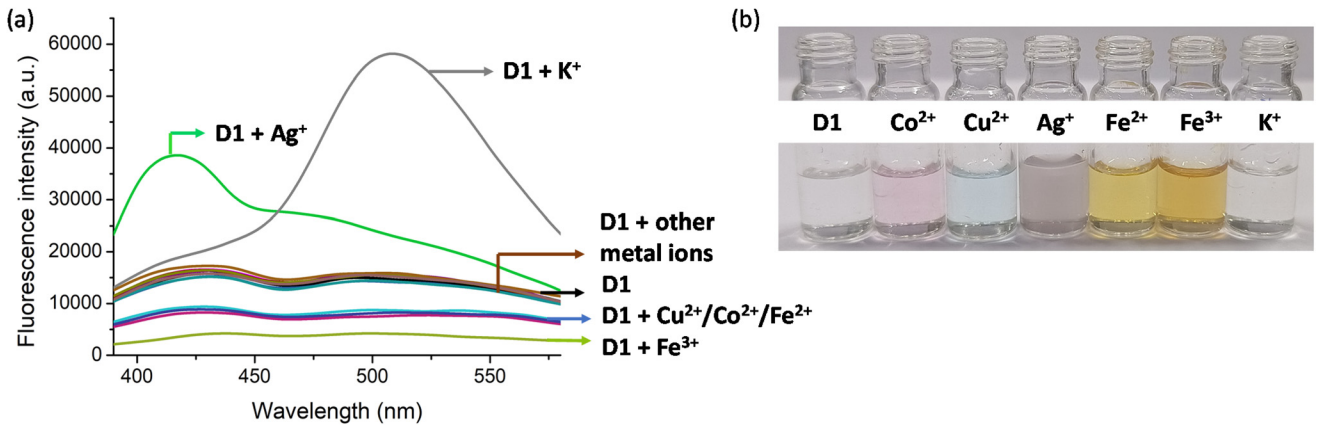

Fig. 4 (a) The fluorescence spectra of **D1** (3 mg mL^{-1}) with different metal ions (50 μM) obtained with an excitation wavelength of 350 nm and an excitation and emission slit width of 20 nm, and (b) a photographic image of **D1** (3 mg mL^{-1}) in the presence of Ag^+, Cu^{2+}, Co^{2+}, Fe^{2+}, Fe^{3+} and K^+ (0.5 mM) viewed under normal light.

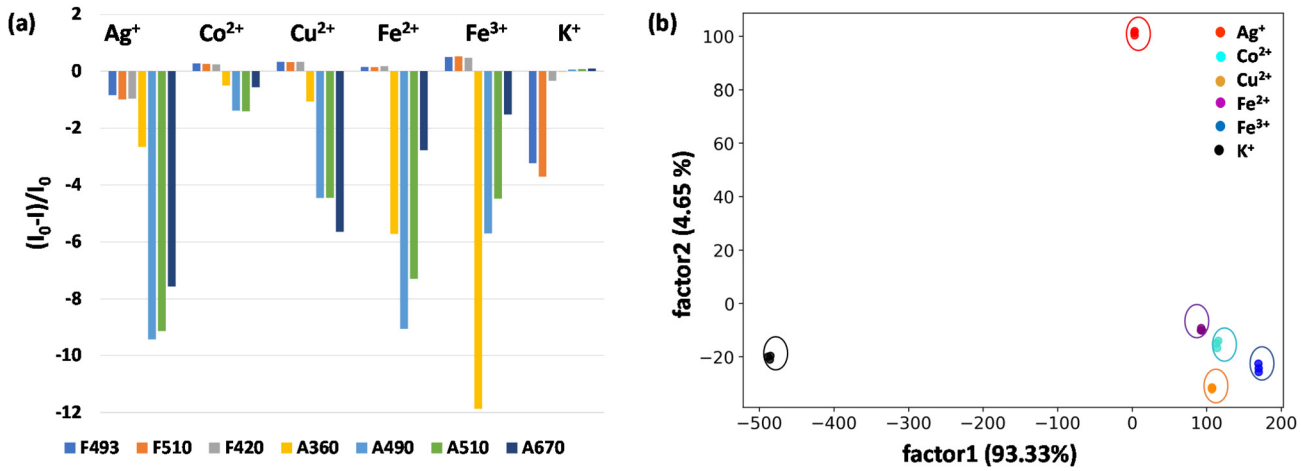

Fig. 5 (a) The absorption and fluorescence response patterns of six metals with **D1** and (b) a LDA plot obtained from the absorbance and fluorescence responses of **D1** with Ag^+, Cu^{2+}, Co^{2+}, Fe^{2+}, Fe^{3+} and K^+.

crete sensor array output and clear separation of clusters validating the application of **D1** as a multi-analyte sensor. The sensitivity of the sensor **D1** was also studied in nanomolar concentrations of metal ions. The LDA plot obtained for this is shown in Fig. S22.† The clear separation and clustering of the analytes were consistent even at these low concentrations. This proves that the polymer **D1** is efficient at detecting trace levels of metal ions. The LOD (limit of detection) of **D1** for the detection of various metal ions, namely, Co^{2+}, Cu^{2+}, Fe^{2+}, Fe^{3+}, Ag^+ and K^+, was also determined. For this, an aqueous solution of **D1** (1 mg mL^{-1}) was made and this was titrated with different metal ions. From the fluorescence spectra recorded, the LOD was calculated using the equation, LOD = $3\sigma/K$, where σ denotes the standard deviation of the sensor alone and K denotes the slope of the regression curve obtained from the plot of fluorescence intensity with concentration of metal ions (Fig. S23–S28†). Hence, the LOD obtained was 4.05 nM for Co^{2+}, 5.01 nM for Cu^{2+}, 1.40 nM for Fe^{2+}, 4.67 nM for Fe^{3+}, 4.48 nM for Ag^+ and 1.02 nM for the K^+ ion. The obtained LODs were within the nanomolar range, which is consistent with the data acquired *via* LDA, which again proves the sensitivity of the sensor and reliability of the data procured.

Conclusions

In conclusion, a simple and efficient strategy was put forward for the development of water-soluble fluorescent polymers. The polymers synthesised were: (a) **D1**, with a dansyl tag and (b) **N1**, with a naphthyl tag. The synthetic strategy for polymerisation incorporates secondary amine functionalities in the backbone, making these polymers soluble in aqueous media. The photophysical studies on these polymers revealed solid-state fluorescence and aggregation induced emission (AIE) behaviour in a water–DMSO mixture. The fluorescence spectra, quantum yield, DLS, and lifetime measurements also suggested the aggregate formation. The metal detection capability of the polymers was studied and this revealed that **N1** was not specific towards any specific metal whereas **D1** produced distinguishable optical signals with six metal ions, namely Cu^{2+}, Co^{2+}, Ag^+, K^+, Fe^{2+} and Fe^{3+}. In view of the discrete spectral behaviour, linear discriminant analysis (LDA) was performed to determine its applicability as a sensor array. In doing so, the six metal ions gave clearly distinguishable clusters with high-level dispersion of output data. Additionally, the addition of Ag^+, Cu^{2+}, Co^{2+}, Fe^{2+}, and Fe^{3+} to **D1** produced discrete colours (Ag^+ purple, Cu^{2+} blue, Co^{2+} pink, Fe^{2+} dark yellow, and Fe^{3+} light yellow), making it a visual sensor for these ions. Taken together, this work proposes a method for the synthesis of water-soluble fluorescent polymers for the discrimination of Cu^{2+}, Co^{2+}, Ag^+, K^+, Fe^{2+} and Fe^{3+} ions, making it suitable for use as a multianalyte sensor. Alongside, we are also exploring the application of the polymer for light emitting diode (LED) and bioimaging applications.

Experimental section

Materials used

All chemicals used in this work were procured from TCI, Sigma Aldrich and Spectrochem.

Instrumentation

The fluorescence measurements were performed using the PerkinElmer FL 6500 instrument and UV using the BioTek EPOCH2 microplate reader. A PerkinElmer STA (Simultaneous Thermal Analyser) 8000 was used for TG DTA measurements. A Carl Zeiss Gemini SEM 300 scanning electron microscope equipped with 2 000 000× magnification and 0.8 nm resolution at 15 kV, and 1.3 nm at 1 kV was used to record the SEM images. The Fluorocube – Life Time System from JOBIN-VYON M/S was used for the time-correlated single photon counting (TCSPC) analysis to obtain the lifetime of the sample.

Synthetic procedure

The synthesis of the polymer started with the reaction of dansyl chloride/2-(bromomethyl)naphthalene reacting with diethanol amine in the presence of triethylamine (TEA) as a base and dichloromethane (DCM) as a solvent. The product obtained was then treated with chloroacetyl chloride in DCM solvent with a TEA base to get the chloroacetylated product. This was then treated with 1,3-propane diamine for 12 hours. The solid obtained was then washed multiple times with acetone and ethylacetate to remove any impurities. The solid was then dried and stored at room temperature.

Quantum yield calculation

The quantum yield was calculated using the following equation:

$$Q_R = Q_S \frac{I_S}{I_R} \frac{A_R}{A_S} \frac{{\eta_S}^2}{{\eta_R}^2}$$

where Q_S and Q_R represent the quantum yield of the sample and the reference, respectively, I_S and I_R represent the integrated area under the emission spectra of the sample and the reference, A_R and A_S represent the absorption of the reference and the sample and η represents the refractive index of the medium. The reference taken was quinine sulphide with a quantum yield of 0.54.

Procedure for fluorescence and absorption analysis

The stock solution of the polymers, **D1** and **N1**, was made at 3 mg mL^{-1} in water. The metal ion solutions of Al^{3+}, Zn^{2+}, Cd^{2+}, Pb^{2+}, Fe^{2+}, Fe^{3+}, Mn^{2+}, Na^{+}, K^{+}, Co^{2+}, Cu^{2+}, Ni^{2+}, Ag^{+}, Ca^{2+} and Hg^{2+} were prepared at 5 mM in water and the required amounts were pipetted out into the cuvette for fluorescence and absorption analysis. For solid state fluorescence, the solid sample was mounted in the sample holder and the absorption and emission spectra were recorded. For solid state microscopy images, the polymer sample was placed on a glass plate and filters with different excitation/emission values (DAPI, 345/455 nm; FITC,494/518 nm; TRITC,555/580 nm; and CY3,550/565 nm) were shon for 200 milliseconds on the sample.

Author contributions

M. P. conceived the concept for the water soluble non-conjugated fluorescent polymers for aggregation induced emission, solid-state fluorescence, and sensor array applications. M. P. and A. J. conceived the molecular design and synthetic protocols. A. T. and A. J. carried out the synthesis, characterization, and fluorescence analysis. A. J. and M. P. analysed the data and wrote the paper.

Conflicts of interest

There are no conflicts to declare.

Acknowledgements

The Indian Institute of Technology Palakkad, India; Ramanujan Fellowship (SB/S2/RJN-145/2017), Science and Engineering Research Board, Department of Science and Technology, India; Scheme for Transformational and Advanced Research in Sciences (MoE/STARS1/293), Ministry of Education, India; Core Research Grant (CRG/2019/002495), Science and Engineering Research Board, Department of Science and Technology, India; the Central Instrumentation Facility (CIF) at the Indian Institute of Technology Palakkad, Indian Institute of Technology Madras and Bharathiar University are acknowledged for the analytical instrumentation support. We thank Athul S B for his support on linear discriminant analysis and Revathy S for the fluorescence microscopy images.

References

1 S. Sengupta, D. Eavarone, I. Capila, G. Zhao, N. Watson, T. Kiziltepe and R. Sasisekharan, *Nature*, 2005, **436**, 568–572.
2 P. Sood, K. B. Thurmond, J. E. Jacob, L. K. Waller, G. O. Silva, D. R. Stewart and D. P. Nowotnik, *Bioconjugate Chem.*, 2006, **17**, 1270–1279.
3 C. Zhu, L. Liu, Q. Yang, F. Lv and S. Wang, *Chem. Rev.*, 2012, **112**, 4687–4735.
4 W. Nasomphan, P. Tangboriboonrat, S. Tanapongpipat and S. Smanmoo, *J. Fluoresc.*, 2014, **24**, 7–11.
5 Y. Cheng, P. Jiang, S. Lin, Y. Li and X. Dong, *Sens. Actuators, B*, 2014, **193**, 838–843.
6 X. Feng, L. Liu, S. Wang and D. Zhu, *Chem. Soc. Rev.*, 2010, **39**, 2411–2419.
7 N. Alizadeh, A. Akbarinejad, S. Hosseinkhani and F. Rabbani, *Anal. Chim. Acta*, 2019, **1084**, 99–105.
8 V. Kumar, B. Maiti, M. K. Chini, P. De and S. Satapathi, *Sci. Rep.*, 2019, **9**, 1–10.
9 S. Zhu, Y. Song, J. Shao, X. Zhao and B. Yang, *Angew. Chem., Int. Ed.*, 2015, **54**, 14626–14637.
10 A. Balamurugan and H. Lee, *Macromolecules*, 2015, **48**, 1048–1054.
11 A. Rostami and M. S. Taylor, *Macromol. Rapid Commun.*, 2012, **33**, 21–34.
12 M. A. Palacios, Z. Wang, V. A. Montes, G. V. Zyryanov and P. Anzenbacher Jr., *J. Am. Chem. Soc.*, 2008, **130**, 10307–10314.
13 Z. Yan, Y. Cai, J. Zhang and Y. Zhao, *Measurement*, 2022, **187**, 110355.
14 W. Xu, C. Ren, C. L. Teoh, J. Peng, S. H. Gadre, H.-W. Rhee, C.-L. K. Lee and Y.-T. Chang, *Anal. Chem.*, 2014, **86**, 8763–8769.
15 X. Shen, Y. Shi, B. Peng, K. Li, J. Xiang, G. Zhang, Z. Liu, Y. Chen and D. Zhang, *Macromol. Biosci.*, 2012, **12**, 1583–1590.

16 S. Chen, J. Liu, Y. Liu, H. Su, Y. Hong, C. K. W. Jim, R. T. K. Kwok, N. Zhao, W. Qin, J. W. Y. Lam, *et al.*, *Chem. Sci.*, 2012, **3**, 1804–1809.
17 Y. Liu, Y. Tang, N. N. Barashkov, I. S. Irgibaeva, J. W. Y. Lam, R. Hu, D. Birimzhanova, Y. Yu and B. Z. Tang, *J. Am. Chem. Soc.*, 2010, **132**, 13951–13953.
18 H. Kobayashi, M. Ogawa, R. Alford, P. L. Choyke and Y. Urano, *Chem. Rev.*, 2010, **110**, 2620–2640.
19 D. W. Domaille, E. L. Que and C. J. Chang, *Nat. Chem. Biol.*, 2008, **4**, 168–175.
20 Z. Zhao, H. Zhang, J. W. Y. Lam and B. Z. Tang, *Angew. Chem., Int. Ed.*, 2020, **59**, 9888–9907.
21 J. Huang, N. Sun, P. Chen, R. Tang, Q. Li, D. Ma and Z. Li, *Chem. Commun.*, 2014, **50**, 2136–2138.
22 B. S. Richards and K. R. McIntosh, *Prog. Photovolt.: Res. Appl.*, 2007, **15**, 27–34.
23 K. Li, T.-B. Ren, S. Huan, L. Yuan and X.-B. Zhang, *J. Am. Chem. Soc.*, 2021, **143**, 21143–21160.
24 J. Mei, N. L. C. Leung, R. T. K. Kwok, J. W. Y. Lam and B. Z. Tang, *Chem. Rev.*, 2015, **115**, 11718–11940.
25 Y. Hong, J. W. Y. Lam and B. Z. Tang, *Chem. Commun.*, 2009, **29**, 4332–4353.
26 F. Würthner, *Angew. Chem., Int. Ed.*, 2020, **59**, 14192–14196.